Scripta Materialia 183 (2020) 45–49

Contents lists available at ScienceDirect

Scripta Materialia

journal homepage: www.elsevier.com/locate/scriptamat

A chemo-mechanical grain boundary model and its application to understand the damage of Li-ion battery materials

Yang Bai[a], Kejie Zhao[b], Yao Liu[a], Peter Stein[a], Bai-Xiang Xu[a,*]

[a] Mechanics of Functional Materials Division, Department of Materials Science, TU,Otto-Berndt-Straße 3 Darmstadt, Germany
[b] School of Mechanical Engineering, Purdue University, West Lafayette, IN 47907, USA

ARTICLE INFO

Article history:
Received 10 December 2019
Revised 6 March 2020
Accepted 11 March 2020

Keywords:
Grain boundary
Fragmentation
Ion transport
NMC particles
Crack propagation

ABSTRACT

Although the unique mechanical and transport features of grain boundaries (GBs) in polycrystalline ion conductors have been recognized, the understanding of the chemo-mechanical interplay and its impact is insufficient. We present a coupled GB model which includes both the damage-dependent across-grain transport and a mechanical cohesive zone law. 3D simulations on $LiNi_xMn_yCo_zO_2$ demonstrate that the chemical process and the mechanical degradation go hand-in-hand: the enhanced intergranular chemical inhomogeneity challenges the GB mechanical strength, while the GB damage influences or even blocks the across-grain transport. Results explain well the experimentally observed features including chemical hot spots and surface layer delamination.

Most ion conductors in energy applications like cathode materials and solid-state electrolytes in Li-ion batteries have polycrystal or multi-grains structure. Compared to the bulk, the grain boundaries (GBs) play thereby significant roles for both their functional and mechanical properties. The unique mechanical and chemical properties of the GBs have been long recognized. For instance, the intergranular cleavage has been widely reported in cathode polycrystalline materials under cyclic charging/discharging. Besides, GBs can influence the ion transport path. However the chemical process and mechanical degradation go hand-in-hand. Their interplay is essential for understanding the functional and mechanical degradation of those materials.

Though the issue we address in this letter is for polycrystalline ion conductors in general, we take the widely used polycrystalline cathode materials $LiNi_xMn_yCo_zO_2$ (NMC) [1,2] as an example. The NMC polycrystal is synthesized as an aggregate of many small grains with the size around 500nm [3,4]. The mechanical strength of the aggregates is determined by the adhesion of grains via Van der Waals interactions. It is thus much weaker than the intrinsic material strength of grains and thus the decohesion of GBs is the major contribution to mechanical degradation. Several numerical efforts have been made to predict the degradation of NMC particles during (de)lithation [4–6]. A cohesive zone model (CZM) was thereby employed to simulate the intergranular fracture within the polycrystal. Later the competition between the energy release rate and fracture resistance during crack growth of NMC material [7] was examined. This showed that the Li extraction can induce material embrittlement, increases the energy release rate, and reduces the fracture toughness. The aforementioned studies provided very useful insights on the crack propagation inside polycrystalline NMC.

However, there are still interesting experimental observations to be explained. One is the prominent lithium inhomogeneities or hot spots, as shown in the transmission X-ray microscopy image by Gent et al. [8], reprinted in Fig. 1b, which can be caused by the inter-grain chemical process [9]. This goes beyond the smooth concentration profile predicted in previous works.

Moreover, the SEM image [4] reprinted in Fig. 1a shows that the fragmentation or disassembly of grains can be restricted to the outside layer of the polycrystal. Such surface layer delamination cannot be predicted by previous models since the calculated diffusion-induced stress favors major radial cracks [10].

Both the hot spots across grains and the surface layer disassembly can be related to chemical interactions between grains. Different than in the grain interior, the lithium concentration at two sides of the GBs can be discontinuous and is merely governed by the chemical potential jumps across GBs [9]. Thus the GB kinetics should be formulated in general with the chemical potential jumps. Sharing similar research interest with ours, Singh and Pal [11] proposed a chemo-mechanical GB model in more recent work. Nevertheless the GB transport is formulated with respect to the concentration jump across GBs, which is suitable for the case of dilute solution. Their two-dimensional results of multi-grains do

* Corresponding author.
E-mail address: xu@mfm.tu-darmstadt.de (B.-X. Xu).

https://doi.org/10.1016/j.scriptamat.2020.03.027
1359-6462/

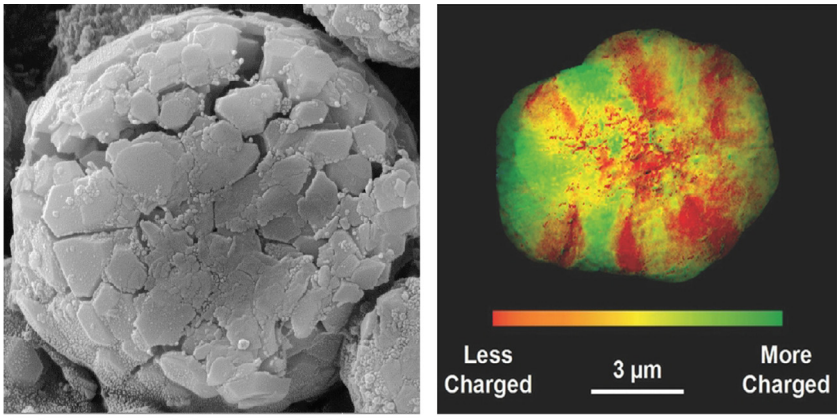

Fig. 1. (a) SEM image of cracks in a NMC particle after the first cycle of charge/discharge (Reproduced with permission from Sun et al. [4]. Copyright 2016 by Elsevier), (b) the elemental mapping from *ex situ* transmission X-ray microscopy (Reproduced with permission from Gent et al. [8]. Copyright 2016 by Wiley Online Library).

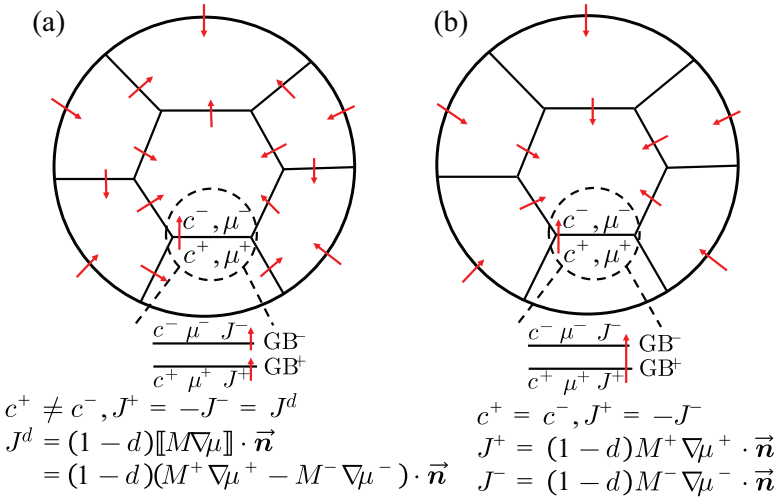

Fig. 2. Illustration of the GB models with (a) and without (b) the across-grain boundary transport.

not show the prominent chemical inhomogeneity observed in experiments, indicating the requirement of a more general GB kinetics. This chemical inhomogeneity resembles the mechanical displacement discontinuity due to GB delamination. Furthermore, if GBs are separated wide enough, the flux across them can even be switched off. Thus the mechanical damage of GBs should be considered in modeling the across-GB transport. The two mentioned issues can lead in the aggregate a highly inhomogeneous concentration distribution which deviates from the classical core-shell type smooth varying concentration profile. The enhanced inhomogeneity is further expected to change the diffusion-induced stress distribution and ultimately the fracture path. In the following, we present a chemo-mechanical grain boundary model and simulations for three-dimensional polycrystalline NMC particles. We contrast the simulated fragmentation patterns and the concentration distribution for cases with and without GB transport, and conclude that the former case leads to results much closer to experimental observations. Besides, we find the anisotropy of elasticity and chemical strain can slightly retard the damage once the GB transport is regarded.

In this letter, we present a chemo-mechanical model, which includes the damage-dependent across-GB transport for lithium transport, and also the cohesive traction-separation law for mechanical degradation. The model is illustrated in Fig. 2, contrasted with a counterpart without the across-GB transport. The ion flux across the GBs is defined as

$$J^+ = -J^- = J^d, \quad J^d = (1-d)\left[M^+\nabla\mu^+ - M^-\nabla\mu^-\right]\cdot\vec{\mathbf{n}} \tag{1}$$

where J, M and μ indicate the normal ion flux, the mobility and the chemical potential, respectively. ∇ is the gradient operator. The superscripts + and - indicate the parameters defined on the two sides of each GB, respectively. The variable d represents the damage state of the GB, which is related to the interface separation in the later context. Any variable with the superscript d denotes that this quantity is damage-dependent. Accordingly, J^d is the damage-dependent flux across the GB. Mass conservation is guaranteed by the first expression in Eq. 1. Once complete failure occurs, namely for $d = 1$, the flux at the GB is cut off. The ion diffusion along the GB is beyond the present work and will be addressed in the future. As for the mechanical part, the continuity equation reads,

$$T_n^+ = T_n^- = T_n(\Delta_n, \Delta_t), \quad T_t^+ = T_t^- = T_t(\Delta_n, \Delta_t) \tag{2}$$

where T_n, T_t are the normal and tangential traction, respectively. Thereby Δ_n, Δ_t are the normal and tangential interface separation, respectively. According to Refs. [12,13], the traction-separation law can be derived from a potential, i.e., $T_n(\Delta_n, \Delta_t) = \delta\Psi_{\mathrm{CZM}}/\delta\Delta_n$ and $T_t(\Delta_n, \Delta_t) = \delta\Psi_{\mathrm{CZM}}/\delta\Delta_t$. The potential Ψ_{CZM} for a mixed-mode

Table 1
Material parameters of $LiNi_xMn_yCo_zO_2$ (NMC).

Name	Symbol and unit	Value
Diffusion coefficient	D [m^2s^{-1}]	7.0×10^{-15}
Max. conc. of NMC particle	C_{max} [mole m^{-3}]	38320
Youngs modulus	E [GPa]	140
Poisson coefficient	ν [-]	0.3
Partial molar volume	Ω [m^3 mol^{-1}]	4.566×10^{-6}
Fracture energy	ϕ_n, ϕ_t [J m^{-2}]	2
Cohesive strength	σ_{max}, τ_{max} [MPa]	100
Non-ideality parameter	χ [-]	2.0
Applied C-rate	-	1C

fracture is thereby expressed as

$$\Psi_{CZM}(\Delta_n, \Delta_t) = \min(\phi_n, \phi_t) + \left[\Gamma_n\left(1 - \frac{\Delta_n}{\Delta_t}\right)^{\alpha}\left(\frac{m}{\alpha} + \frac{\Delta_n}{\delta_n}\right)^{m} + \langle \phi_n - \phi_t \rangle\right] \cdot \left[\Gamma_t\left(1 - \frac{|\Delta_t|}{\delta_t}\right)^{\beta}\left(\frac{n}{\beta} + \frac{|\Delta_t|}{\delta_t}\right)^{n} + \langle \phi_t - \phi_n \rangle\right], \quad (3)$$

where ϕ_n and ϕ_t are the normal and tangential fracture energies, and where δ_n and δ_t further represent the final crack opening widths in the normal and tangential direction, respectively. The symbol $\langle \cdot \rangle$ denotes the *Macaulay bracket*, namely $\langle x \rangle = 0$ if $x < 0$, and $\langle x \rangle = x$ if $x \geq 0$. Whereby, the damage variable is expressed as $d = \langle \Delta_{eff} - \Delta_c \rangle / (\delta_{eff} - \Delta_c)$. $\Delta_{eff} = \sqrt{\Delta_n^2 + \Delta_t^2}$ and $\delta_{eff} = \sqrt{\delta_n^2 + \delta_t^2}$ are the effective separation and crack opening width for the mixed case, and Δ_c denotes the critical separation for damage initiation.

For the grain interior, we employ a mechanically coupled diffusion model used in our previous publications [14–17]. The mechanical equilibrium and the ion diffusion equation are

$$\nabla \cdot \boldsymbol{\sigma} = \mathbf{0}, \qquad \frac{\partial c}{\partial t} = \nabla \cdot (M \nabla \mu), \quad (4)$$

where $\boldsymbol{\sigma}$ is the Cauchy stress tensor, $M = Dc(1-c)$ describes the concentration-dependent mobility with D being the diffusion coefficient. In a thermodynamic consistent formulation, the chemical potential and the stress can be obtained from the corresponding variational derivatives of the system free energy, i.e., $\mu = \delta\psi/\delta c$, $\boldsymbol{\sigma} = \delta\psi/\delta\mathbf{E}$, with $\mathbf{E}$ being the Green–Lagrange strain tensor. Accordingly, the free energy $\psi = \psi^c + \psi^e$ with the bulk free energy and the elastic energy have the following form:

$$\psi^c = c \ln c + (1-c)\ln(1-c) + \chi c(1-c), \quad (5)$$

$$\psi^e = \det\mathbf{F}^c \left[\frac{K}{2}\left(\frac{\det\mathbf{F}}{\det\mathbf{F}^c} - 1\right)^2 + \frac{G}{2}\left(\bar{I}_1 - 3\right)\right]. \quad (6)$$

Here, χ is a parameter for non-ideal solution, K and G respectively denote the bulk and shear moduli. $\bar{I}_1$ is the first invariant of the right Cauchy–Green deformation tensor. $\det\mathbf{F}$ and $\det\mathbf{F}^c$ are the Jacobian determinants of the deformation gradient tensor $\mathbf{F}$ and its chemical part, respectively. Note that the structural transition is neglected.

The finite element software MOOSE [18,19] is applied to implement the outlined model. The Discontinuous Galerkin method is applied for the discontinuity of displacement and concentration at GBs. Aggregates with radius $R = 5\mu$m comprising 89, 174 and 413 grains are considered separately, to achieve representative statements. The 1C-rate discharge process is applied for all the aggregates. The material properties of NMC are taken from Refs. [6,7,20–23] and listed in Table 1.

We first demonstrate the impact of the across-GB transport between grains on the fracture pattern of the aggregates by comparing the results with and without the across-GB transport, as illustrated in Fig. 2. Thereby the anisotropy of the grains is ignored, its influence is demonstrated in later examples. Fig. 3 compares the concentration and damage fields within the considered aggregates. It can be seen that for all the grain sizes, the across-GB transport results in stronger concentration inhomogeneities, together with noticeable concentration hot spots and higher degrees of interface damage, which is confirmed by the elemental mapping in Fig. 3c resulting from experiments. Furthermore, we can recognize pronounced concentration jumps towards inner grains. These result in a larger volume expansion of the outer grains and hence in a strong strain mismatch along GBs between neighboring grains. Once cracks open up wide enough, the flux between neighboring grains is cut off and the lithium cannot diffuse towards the center of the aggregate. Instead, the lithium will accumulate in the outer grain layer, which can further accelerate the damage of NMC particles. Several small grains are even "squeezed" out from their environment. Moreover, for the case with smaller grain size (higher number of grains), the aggregates experience stronger surface delamination, which can be observed from the SEM image of NMC particles shown in Fig. 3d. We attribute this effect to the shorter interaction distance of the stresses between neighboring grains. In the cases without the across-GB transport, on the other hand, the concentration field varies much smoother along the aggregate's radius. The strain mismatch is hence comparatively small and cracks mainly form in the core of the aggregate, similar to the results shown in the mentioned literature. Subsequently, several small cracks will grow away from the main crack. The surface delamination is thereby suppressed due to the absence of surface layer blocking effects. On the other hand, experiments also confirm that by adding a glue-nanofiller between the grains [24] or performing nanoscale surface treatment of grains with a mixed ethanol solution [25], the interfacial bonding can be enhanced and the cracks can be suppressed. Thereby, both the GBs with stronger mechanical strength (namely a higher fracture energy) and the GBs with better ion conductivity (resulting in a stronger across-GB transport with fewer concentration jumps) are suggested to alleviate cracks and improve the chemo-mechanical performance of the particle.

We now analyze the influence of the anisotropy of elasticity and chemical strain on the crack patterns of NMC particles, and thereby the GB model with across-GB transport is regarded. The elastic strain energy is treated as $\psi^e = \frac{1}{2}\boldsymbol{E} : \mathbb{C} : \boldsymbol{E}$, where $\boldsymbol{E}$ denotes the Green–Lagrange strain tensor and where $\mathbb{C}$ represents the anisotropic elasticity tensor [26]. Following [27], we employ a stiffness of the in-plane axis that is two times larger than that of the out-of-plane axis. Thus the Young's modulus of different axes is considered as $E_{xx} = E_{yy} = 2E_{zz} =$ 140GPa locally. In addition, the anisotropic eigenstrain is introduced as $c\Omega/3\bar{\boldsymbol{I}}$ for the anisotropic volume expansion, where $\bar{\boldsymbol{I}} = \begin{bmatrix}-0.02 & -0.02 & 0.01 & 0 & 0 & 0\end{bmatrix}$ is an anisotropic tensor in Voigt notation. Aggregation of randomly oriented grains thus results in macroscopically isotropic properties, whereas the properties of individual grains remain locally anisotropic.

If the aggregate is modeled as a uniform continuum and the across-GB transport is ignored, a domain wall migrates through the aggregate in the radial direction, separating the exterior regions of high concentration from those with a low concentration in the interior. The strain mismatch is concentrated along the concentration gradient, as are the first principal stresses (σ_{sp1}). During initial states of discharge, a tensile stress state is established in the aggregate center, which is relaxed by the formation and the subsequent (low) growth of cracks. The introduction of anisotropy changes the behavior insofar as that the grains now try to expand along their randomly oriented lattice directions. The regular distribution of

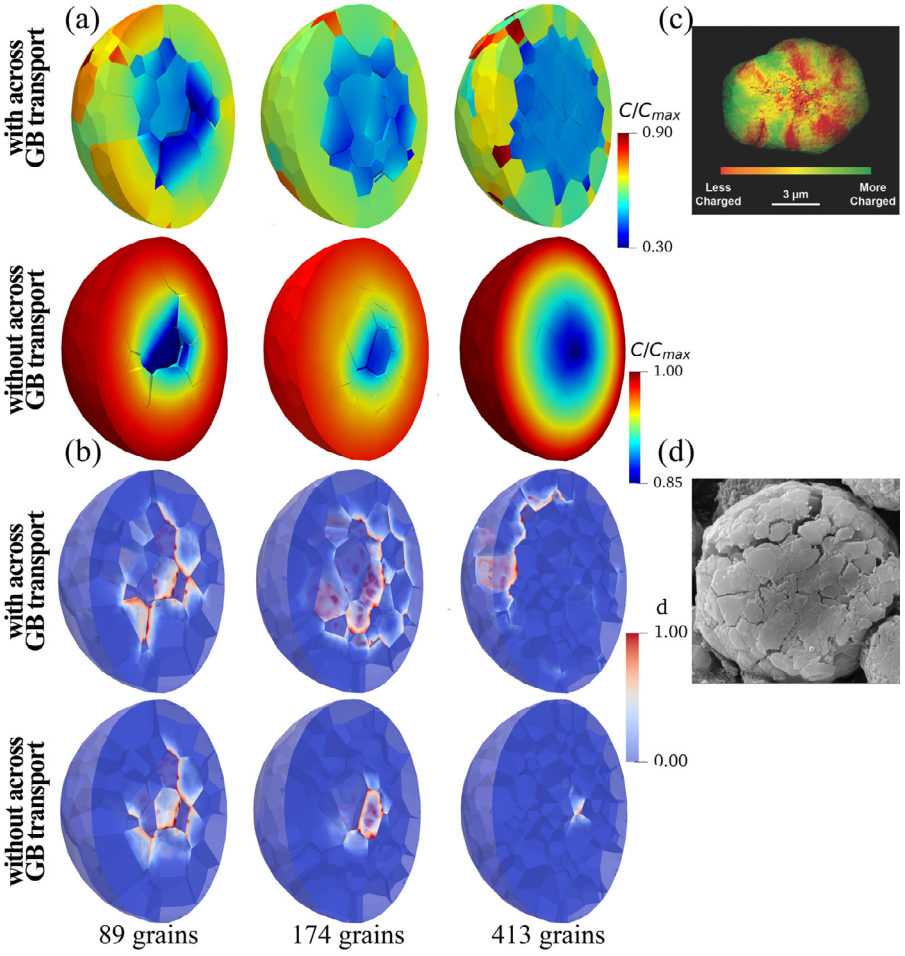

Fig. 3. Comparison of the concentration distribution and the resulting crack patterns between the cases with (a) and without (b) across-GB transport. Concentration hot spots and surface layer delamination are visible in the cases with this interaction, which are confirmed by (c) reprint of the elemental mapping from *ex situ* transmission X-ray microscopy (Reproduced with permission from Gent et al. [8]. Copyright 2016 by Wiley Online Library), (d) reprint of cracks in NMC particle after the first cycle of charge/discharge using SEM imaging (Reproduced with permission from Sun et al. [4]. Copyright 2016 by Elsevier).

σ_{sp1} along phase interfaces is now replaced by a scattered distribution, and the stresses show a much wider range compared to the isotropic case. In particular, the outermost grains show a "local" core-shell distribution of stresses, with compressive stresses in the outer layers and strong tensile stresses towards the center of the aggregate. This induces a strong strain mismatch along the GBs. The cracks formed at the aggregate center are thus "pulled" away from the interior of the grain agglomerate. Along the main crack branches, the stress relaxation results in a redistribution of ions due to stress-assisted diffusion effects [28].

However, the behavior changes once the across-GB transport is included, although the scattered distribution of σ_{sp1} is sustained. During the initial stages of discharge, cracks nucleate in the aggregate center and are pulled outward by the strain mismatch in its outer layers. The crack growth thereby proceeds faster than the diffusion process. Consequently, the ion transport towards the aggregate center is cut off, resulting in the aforementioned surface layer blocking effect. The strong strain mismatch between the outermost grains and their neighbors towards the aggregate center thereby attracts the cracks to radiate outwards. Concurrently, some of the outermost grains de-laminate from the agglomerate. The introduction of the piecewise anisotropic elastic behavior appears to reduce the severity of this damaging process. The anisotropic chemical expansion of neighbor grains appears to accommodate the strain mismatch between neighbor grains. The distribution of σ_{sp1} is now shifted towards a more concentric arrangement, and the magnitude of stresses is slightly reduced. As a result, the amount of damage in the grain aggregate is slightly reduced, as shown in Fig. 4.

To further understand and summarize the difference, we determined the damage fraction as shown in Fig. 4c. The damage fraction is defined as $\frac{1}{A_\Gamma}\int_\Gamma d\,\mathrm{dA}$, where Γ denotes the GB surface area. It is clear that the across-GB transport enhances significantly the damage for both cases with and without anisotropy. Nevertheless, the anisotropy plays a different role depending on the fact whether the across-GB transport is regarded or not. If this interaction is ignored, the anisotropy obviously promotes the damage development, as it is shown by the comparison between the solid red line and dashed red line. This is in contrast to the results if the across-GB transport is considered, as shown by the comparison of the black solid and dashed lines. More particularly, the anisotropy retards the damage development slightly. This is likely due to the random/scattered nature of the anisotropy mismatch, which partially relaxes the mismatch strain induced by the hot spots.

A chemo-mechanical damage model has been developed to study the fracture of cathode materials with polycrystalline structure. It includes the across-GB transport and the cohesive traction-separation law along GBs. Simulation results of NMC polycrystals indicate that if the diffusion of the aggregate is modeled as a single homogeneous particle, the diffusion-induced damage is comparable to that induced by the anisotropy mismatch. However, this significantly underestimates the damage since the model cannot reproduce the enhanced chemical inhomogeneity and thus the

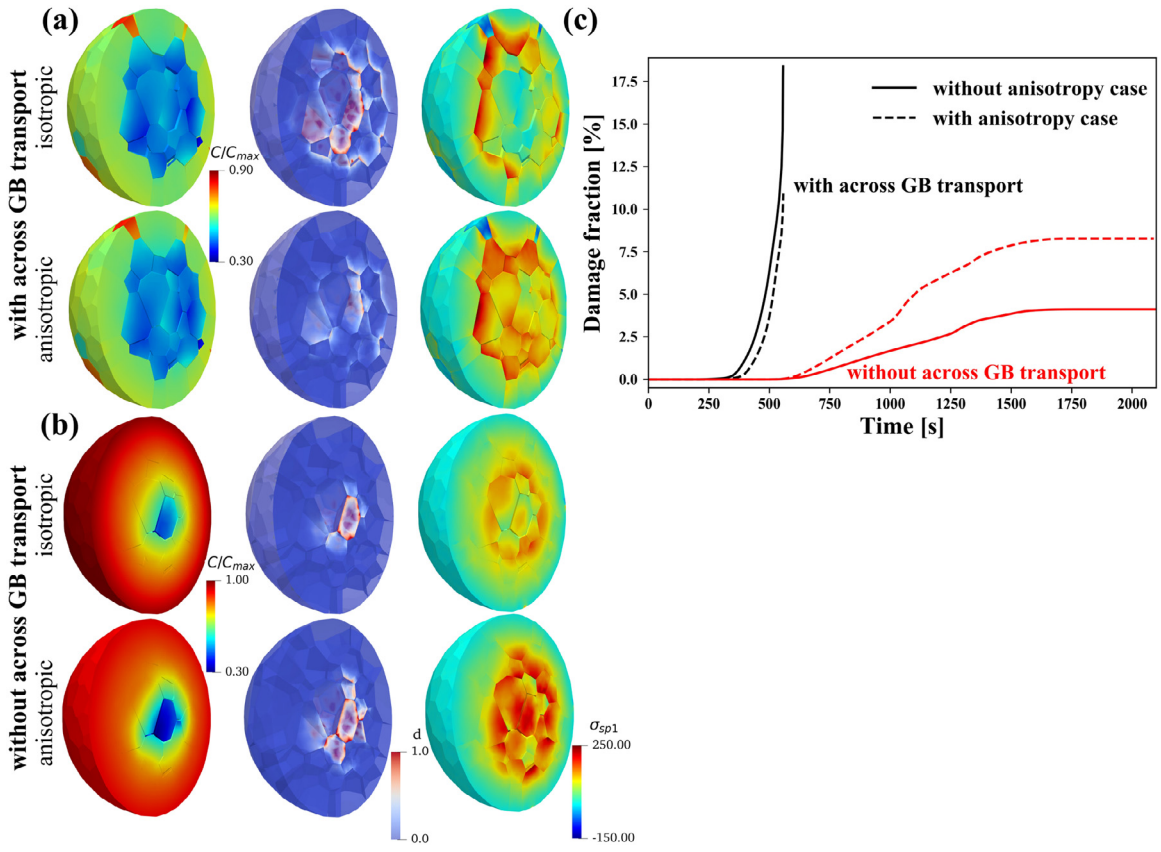

Fig. 4. Influence of the anisotropy on the distribution of the concentration, damage state, and the maximum principal stress σ_{sp1} (MPa) in aggregates with (a) and without (b) across-GB transport, (c) the accumulated damage within an aggregate (with 174 grains) for the cases with/without anisotropy or across-GB transport.

surface layer delamination. For this purpose, one should consider the across-GB transport and its dependency on the interface damage. Interestingly, the anisotropy of the elasticity and chemical strain tends to retard the damage induced by this transport.

Declaration of Competing Interest

The authors declare that they have no known competing financial interests or personal relationships that could have appeared to influence the work reported in this paper.

Acknowledgment

The authors gratefully acknowledge the computing time granted on the Hessian High-Performance Computer “Lichtenberg”.

Supplementary materials

Supplementary material associated with this article can be found, in the online version, at doi:10.1016/j.scriptamat.2020.03.027

References

[1] C. Daniel, D. Mohanty, J. Li, D. L. Wood, in: AIP, pp. 26–43.
[2] J.E. Harlow, X. Ma, J. Li, E. Logan, Y. Liu, N. Zhang, L. Ma, S.L. Glazier, M.M.E. Cormier, M. Genovese, S. Buteau, A. Cameron, J.E. Stark, J.R. Dahn, J. Electrochem. Soc. 166 (2019) A3031–A3044.
[3] D.J. Miller, C. Proff, J. Wen, D.P. Abraham, J. Bareño, Adv. Energy Mater. 3 (2013) 1098–1103.
[4] G. Sun, T. Sui, B. Song, H. Zheng, L. Lu, A.M. Korsunsky, Extreme Mech. Lett. 9 (2016) 449–458.
[5] Y. Zhang, C. Zhao, Z. Guo, Int. J. Mech. Sci. 155 (2019) 178–186.
[6] R. Xu, L. de Vasconcelos, J. Shi, J. Li, K. Zhao, Exp. Mech. 58 (2018) 549–559.
[7] R. Xu, K. Zhao, J. Mech. Phys. Solids 121 (2018) 258–280.
[8] W.E. Gent, Y. Li, S. Ahn, J. Lim, Y. Liu, A.M. Wise, C.B. Gopal, D.N. Mueller, R. Davis, J.N. Weker, J.-H. Park, D. Seok-Kwang, C. William, Adv. Mater. 28 (2016) 6631–6638.
[9] Y. Zhao, L.R. De Jesus, P. Stein, G.A. Horrocks, S. Banerjee, B.X. Xu, RSC Adv. 7 (2017) 41254–41264.
[10] H.-H. Sun, A. Manthiram, Chem. Mater. 29 (2017) 8486–8493.
[11] A. Singh, S. Pal, Int. J. Plast. (2019).
[12] K. Park, G.H. Paulino, J.R. Roesler, J. Mech. Phys. Solids 57 (2009) 891–908.
[13] K. Park, G.H. Paulino, Eng. Fract. Mech. 93 (2012) 239–262.
[14] Y. Zhao, P. Stein, B.X. Xu, Comput. Methods Appl. Mech. Engrg. 297 (2015) 325–347.
[15] Y. Bai, Y. Zhao, W. Liu, B.X. Xu, J. Power Sources 422 (2019) 92–103.
[16] Y. Zhao, P. Stein, Y. Bai, M. Al-Siraj, Y. Yang, B.X. Xu, J. Power Sources 413 (2019) 259–283.
[17] B.-X. Xu, Y. Zhao, P. Stein, GAMM-Mitteilungen 39 (2016) 92–109.
[18] D. Gaston, C. Newman, G. Hansen, D. Lebrun-Grandie, Nucl. Eng. Des. 239 (2009) 1768–1778.
[19] B.S. Kirk, J.W. Peterson, R.H. Stogner, G.F. Carey, Eng. Comput. 22 (2006) 237–254.
[20] L. de Vasconcelos, N. Sharma, R. Xu, K. Zhao, Exp. Mech. 59 (2019) 337–347.
[21] R. Xu, H. Sun, L.S. de Vasconcelos, K. Zhao, J. Electrochem. Soc. 164 (2017) A3333–A3341.
[22] K. Min, E. Cho, Phys. Chem. Chem. Phys. 20 (2018) 27115–27124.
[23] Y. Bai, C. Dong, Z. Liu, Compos. Struct. 128 (2015) 54–69.
[24] H. Kim, S. Lee, H. Cho, J. Kim, J. Lee, S. Park, S.H. Joo, S.H. Kim, Y.-G. Cho, H.K. Song, et al., Adv. Mater. 28 (2016) 4705–4712.
[25] H. Kim, M.G. Kim, H.Y. Jeong, H. Nam, J. Cho, Nano Lett. 15 (2015) 2111–2119.
[26] T. Belytschko, W.K. Liu, B. Moran, K. Elkhodary, Nonlinear Finite Elements for Continua and Structures, John Wiley & Sons, 2013.
[27] H. Sun, K. Zhao, J. Phys. Chem. C 121 (2017) 6002–6010.
[28] P. Stein, B. Xu, Comput. Methods Appl. Mech. Engrg. 268 (2014) 225–244.